TLR2 Supports γδ T cell IL-17A Response to ocular surface commensals by Metabolic Reprogramming

Wenjie Zhu[1,2#], Xiaoyan Xu[1#*], Vijayaraj Nagarajan[1], Jing Guo[3], Zixuan Peng[1], Amy Zhang[1], Jie Liu[1,4], Mary J. Mattapallil[1], Yingyos Jittayasothorn[1], Reiko Horai[1], Anthony J. St. Leger[5], Rachel R. Caspi[1*]

[1]Laboratory of Immunology, NEI, NIH Bethesda MD 20892, USA

[2]State Key Laboratory of Ophthalmology, Zhongshan Ophthalmic Center, Sun Yat-sen University, Guangzhou, 510060 China

[3]Department of Microbiology and Immunology, Stanford University School of Medicine, Stanford, CA 94305, USA

[4]Current address: Schepens Eye Research Institute, Massachusetts Eye and Ear Infirmary, Harvard Medical School, Boston, MA, 02114

[5]University of Pittsburgh School of Medicine, Departments of Ophthalmology and Immunology, Pittsburgh, PA 15213, USA

# Equal contribution

***Correspondence**: Rachel R. Caspi (caspir@nei.nih.gov) or Xiaoyan Xu (xiaoyan.xu2@nih.gov)

Short title: Metabolic Reprogramming by TLR2 for Ocular IL-17A

Summary: The ocular commensal *Corynebacterium mastitidis* (*C. mast*) induces the IL-17 responses from γδ T cells by activating TLR2 signaling. γδ T cell-intrinsic TLR2 stimulation promotes fatty acid oxidation and increases *IL-17A* transcription, favoring IL-17A responses.

Key words: TLR2, γδ T cells, ocular commensal, FAO, IL-17A

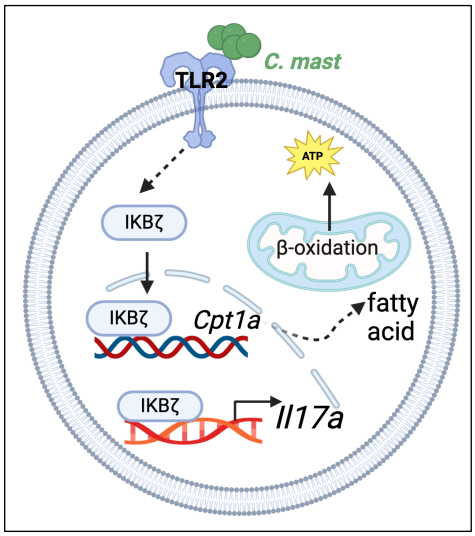

Highlights:

(1) TLR2-deficient mice exhibit reduced γδ T cell responses to ocular commensal bacteria.

(2) γδ T cell-intrinsic TLR2 deficiency causes defects of fatty acid oxidation and IL-17A production in a γδ subset-specific manner.

(3) The transcription factor, IκBζ is upregulated by TLR2 stimulation and supports γδ IL-17A production through fatty acid oxidation.

ABSTRACT

The ocular surface is a mucosal barrier tissue colonized by commensal microbes, which tune local immunity by eliciting IL-17 from conjunctival γδ T cells to prevent pathogenic infection. The commensal *Corynebacterium mastitidis* (*C. mast*) elicits protective IL-17 responses from conjunctival Vγ4 T cells through a combination of γδ TCR ligation and IL-1 signaling. Here, we identify Vγ6 T cells as a major *C. mast*-responsive subset in the conjunctiva and uncover its unique activation requirements. We demonstrate that Vγ6 cells require not only extrinsic (via dendritic cells) but also intrinsic TLR2 stimulation for optimal IL-17A response. Mechanistically, intrinsic TLR2 signaling was associated with epigenetic changes and enhanced expression of genes responsible for metabolic shift to fatty acid oxidation to support *Il17a* transcription. We identify one key transcription factor, IκBζ, which is upregulated by TLR2 stimulation and is essential for this program. Our study highlights the importance of intrinsic TLR2 signaling in driving metabolic reprogramming and production of IL-17A in microbiome-specific mucosal γδ T cells.

INTRODUCTION

An immunological balance between microbes and mucosal barrier tissues is required to ensure tissue health and homeostasis. Specifically, immune cells must mount a response that limits the outgrowth of microbes from becoming pathobionts without causing immunopathology. The cytokine interleukin (IL)-17 plays a critical role in this process. IL-17 is required at virtually every mucosal site in the body to limit outgrowth of bacteria and fungi in the steady-state (Li et al., 2019). Humans and mice deficient in production of IL-17A and F experience severe and life-threatening infections (Acosta-Rodriguez et al., 2007).

Regulation of IL-17 production in CD4+ αβ T cells relies on a combination of T cell receptor stimulation and signals from proinflammatory cytokines like IL-23, IL-1β, and IL-6 (Gomez-Rodriguez et al., 2014; Zhou et al., 2007). Regulation of IL-17 production in unconventional lymphoid cells, such as invariant natural killer T cells (iNKT), innate lymphoid cells (ILC), and γδ T cells, which often have critical biological functions at mucosal barrier sites, is less well-understood. Although IL-1β signaling is required by iNKT and γδ T cells for IL-17 production (Sutton et al., 2009), TCR ligation is essential for an optimal response (Duan et al., 2010). We as well as others have demonstrated the critical role of IL-17 produced by unconventional T cells in autoimmunity and mucosal host defense, highlighting the importance of mechanisms that govern the effector functions of these cells (Edwards et al., 2020; Sherlock et al., 2012; St Leger et al., 2018).

The conjunctiva of the eye is a specialized mucosal tissue responsible for protecting the ocular surface against allergic and infectious insults (Knop and Knop, 2005). Mice deficient in IL-17A and IL-17F are highly susceptible to severe bacterial and fungal infections, including corneal *Candida albicans* infection and the spontaneous outgrowth of *Staphylococcus spp.* (Conti et al., 2014; St Leger et al., 2018). We previously demonstrated that conjunctival γδ T cells are key contributors to the protective IL-17 elicited at the ocular surface by the Gram-positive commensal bacterium, *Corynebacterium mastitidis (C. mast)* (St Leger et al., 2017). In Vγ4 γδ T cells, IL-17A production relied on TCR ligation and IL-1β signaling. Notably, *C. mast* also stimulated IL-17A production in Vγ4-negative γδ T cells, but their identity and the signals they required to induce IL-17A were unclear. Tight control over the production of conjunctival IL-17A is required to both prevent the outgrowth of pathobionts, and to limit bystander damage to the ocular surface, such as occurs in dry eye and other ocular surface diseases (de Paiva et al., 2022; Gadjeva et al., 2010; Suryawanshi et al., 2011). Therefore, understanding how an eye-colonizing microbe stimulates IL-17 in the Vγ4-negative γδ T cell subset will be essential for deciphering how mucosal immune responses are maintained at the ocular surface.

IL-17 responses in γδ T cells can be stimulated indirectly by microbial components which are sensed by toll-like receptors (TLRs) on myeloid cells that produce IL-1β and IL-23, which in turn stimulate IL-17A-producing γδ T cells (γδT17) (Akira and Takeda, 2004). However, γδ T cells themselves express various TLRs, including TLR2, TLR4, TLR6 and TLR9, which can affect their effector functions. For example, direct TLR2 engagement *in vivo* by the synthetic LPS analog Pam3CSK4 enhances γδ T cell proliferation and IL-17 production (Marks et al., 2021; Martin et al., 2009; Reynolds et al., 2010).

In addition to immune activation pathways, the metabolic regulation of γδT17 cells has recently become an area of intense interest. The development and the pro-tumor function of γδT17 cells were shown to be under metabolic control (Cai et al., 2019; Lopes et al., 2021). However, the molecular mechanisms and the role of TLR2 in metabolic programming of these cells are not known. Our study offers to bridge these gaps by elucidating how TLR2 signaling influences IL-17 production through metabolic reprogramming of *C. mast*-specific γδ T cells.

Utilizing TLR2-deficient (TLR2-/-) mice colonized with *C. mast*, we demonstrate that TLR2 expression is essential in both dendritic cells (DCs) and in γδ T cells themselves for optimal IL-17A production. Our findings reveal that intrinsic TLR2 signaling in γδ T cells is linked to activation of the transcription factor IκBζ and causes a metabolic shift to fatty acid oxidation to support IL-17 production. Our findings underscore the significance of TLR2 in the metabolic and immune regulatory pathways of mucosal γδ T cells and highlight its potential as a target for modulating immune responses at mucosal barriers.

RESULTS

TLR2 is required for IL-17A production in response to *C. mast* at the ocular surface

Ocular colonization with the microbe, *C. mast*, results in the expansion of γδT17 cells in the eye draining lymph nodes (DLNs) (St Leger et al., 2017). These cells accumulate in the conjunctiva where their functionality leads to a steady-state, non-pathogenic recruitment of neutrophils to the tissue. Even though TCR stimulation and IL-1β were shown to induce IL-17, the requirement of innate receptors in the production of IL-17 in these cells was still unresolved. Therefore, we focused our attention on the requirement of TLR2 signaling in mucosal γδ T cell IL-17 responses. We ocularly colonized WT or TLR2$^{-/-}$ mice with *C. mast*, as previously reported, and assessed the production of IL-17A in DLNs. We found the percentage of IL-17A positive cells and the mean fluorescence index (MFI) of IL-17A in DLNs were reduced in TLR2$^{-/-}$ mice compared to WT mice (Fig. 1A - B). This was due, in part, to a reduction in proliferation as measured by the expression of Ki67 within DLN γδ T cells (Fig. 1C). There was a concurrent reduction of IL-17 in the γδ T cell compartment of the conjunctiva (Fig. 1D). The effect of the reduction in IL-17 was also observed in the recruitment of neutrophils to the conjunctiva (Fig. 1E).

TLR2 on γδ T cells is required for their IL-17A response to *C. mast in vitro*

TLR2 is expressed on γδ T cells and DCs at inflammatory sites (Mokuno et al., 2000; Oliveira-Nascimento et al., 2012) and is required for microbe-specific IL-17 production, we sought to identify the immune cells that express TLR2 in the context of ocular *C. mast* colonization. Within the conjunctiva, both DCs and γδ T cells express detectable levels of TLR2 after *C. mast* inoculation, suggesting a role for this receptor in *C. mast*-specific IL-17 response (Fig. 2A). In contrast, conjunctival αβ T cells did not express detectable levels of TLR2 regardless of the presence of *C. mast.*

These data prompted the question of whether TLR2 expression is necessary on DCs, γδ T cells, or both for *C. mast*-specific IL-17 response. To address this, we examined co-cultures of WT and TLR2-deficient DCs and γδ T cells in all reciprocal combinations, in the presence or absence of heat-killed C. mast. Stimulation with *C. mast* expectedly enhanced IL-17A production in cultures containing WT DCs and WT γδ T cells. In contrast, TLR2$^{-/-}$ DCs supported a significantly reduced γδ IL-17 response: fewer IL-17A+ γδ T cells, lower MFI of IL-17-positive cells (Fig. S1A), and less secreted IL-17A as measured by ELISA (Fig. S1B). Because DCs activated by TLR2 signals secrete IL-1β and IL-23, needed for γδ T cells to express IL-17A, we measured

the levels of these cytokines in the co-culture supernatants. TLR2$^{-/-}$ DCs produced less IL-1β (but not IL-23) in response to *C. mast* stimulation (Fig. S1C-D), suggesting that diminished IL-1β production by TLR2$^{-/-}$ DCs may have accounted for the reduced IL-17A production by γδ T cells. This was confirmed by the ability of exogenous IL-1β to restore IL-17A production to levels comparable to those observed with WT DCs (Fig. S1E).

Next, we examined the effect of TLR2 deficiency in γδ T cells in their response to *C. mast*. In the presence of WT DCs, TLR2$^{-/-}$ γδ T cells still produced less IL-17A than WT, by flow cytometry and ELISA (Fig. 2B-C), despite undiminished IL-1β and IL-23 (Fig. 2D-E). This indicated that optimal IL-17A production in response to *C. mast* in these cultures required TLR2 expression on both DCs and γδ T cells. While the need for TLR2 on DCs can be explained by their production of IL-1β, endogenous TLR2 expression on γδ T cells is independently needed to support their IL-17 response.

The absence of TLR2 on γδ T cells decreases their IL-17A responses *in vivo*

To study the γδ cell-intrinsic role of TLR2 *in vivo*, we performed adoptive transfer of TLR2-sufficient (WT) or deficient (KO) γδ T cells into TCRδ$^{-/-}$ mice, which lack γδ T cells entirely. Donor γδ T cells were purified by sorting from (*C. mast*–naïve) CD45.1 WT or CD45.2 TLR2$^{-/-}$ mice and were co-transferred at a 1:1 ratio to sublethally irradiated (450 R) TCRδ$^{-/-}$ recipient mice. One week after cell transfer, the recipients were ocularly associated with *C. mast* or PBS as a control, and after another week, we assessed their IL-17A responses (Fig. 3A). In the *C. mast*-unassociated group, both WT and TLR2$^{-/-}$ γδ T cells populated the recipient mice with similar efficiency, indicating that TLR2 is not required for γδ T cell “fitness” over the observation time period (Fig. 3B). However, in mice associated with *C. mast*, TLR2$^{-/-}$ γδ T cells displayed reduced responses compared to the co-transferred WT γδ T cells (Fig. 3B). We observed a lower percentage of IL-17A positive cells, diminished ex-vivo IL-17A production to PMA per cell (MFI), and a lower proportion of proliferating (Ki67^{+}) cells (Fig. 3C-D). These results confirm the cell-intrinsic role of TLR2 on γδ T cells for activation and IL-17A production in response to *C. mast in vivo*.

TLR2$^{-/-}$ Vγ6 cells exhibit a more profoundly impaired response to *C. mast than* Vγ4 cells

The function of γδ T cells in terms of cytokine production is closely linked to their usage of specific TCR repertoires. γδ T cell subsets expressing Vγ1, Vγ4, and Vγ6 (Heilig and Tonegawa’s nomenclature) produce IL-17A (Heilig and Tonegawa, 1986; O'Brien and Born, 2020; Shibata et al., 2007). In our previous study, we identified IL-17A-producing Vγ4 cells at the ocular surface of *C. mast*-colonized mice (St Leger et al., 2017). We also observed a

population of Vγ4– γδ T cells that produced IL-17 but did not characterize their TCR or their requirements for stimulation. We now noted that ocular *C. mast* association increased the number of Vγ1^{-}Vγ4^{-} T cells that produced IL-17A in the conjunctiva (Fig. 4A). Using a TCR-specific antibody (17D1), we identified them as expressing the Vγ6 TCR (Roark et al., 2004) (Fig. 4B). Analysis of eye DLNs revealed the presence of IL-17A^{+} Vγ6 cells even in *C. mast*-naïve mice, but the number of these cells and their IL-17A-producing capacity were considerably increased after C. mast inoculation (Fig. 4C). Notably, expression of TLR2 became significantly elevated on Vγ6 γδ T cells after *C. mast* colonization compared to other populations of γδ T cells (Fig. 4D).

The elevated expression of TLR2 on Vγ6 γδ T cells raised the possibility that TLR2 may have divergent roles in Vγ4 and Vγ6 IL-17A-producing γδ T (γδ T17) cells. We therefore examined the kinetics of IL-17A production by Vγ4 and Vγ6 T cells in the DLNs in response to *C. mast.* The response of Vγ6 cells occurred earlier and was stronger than that of Vγ4 cells, occurring by day 10 in WT mice (Fig. 4E-F) and TLR2 deficiency compromised IL-17A production and proliferation (Ki67) of Vγ6 T cells to a greater extent than that of Vγ4 T cells (Fig. 4G). Together, these data lead to the conclusion that Vγ6 T cells are more dependent on TLR2 signaling than are Vγ4 T cells for their responses to the eye-colonizing commensal.

TLR2 signals regulate the transcriptomic and epigenomic production of IL-17A in Vγ6 cells

To study the basis for the requirement of TLR2 signals in the Vγ6 T subset, we performed RNA-seq on Vγ6 cells sorted from mice prior to and after *C. mast* inoculation (Fig. S2A). The principal component analysis (PCA) plot of the transcriptome revealed distinct clusters formed by WT and TLR2$^{-/-}$ Vγ6 γδ T cells (Fig. 5A). Consistent with observations presented in Figure 4, the Vγ6 T cells from TLR2$^{-/-}$ mice displayed lower expression of *Il17a* -related genes, such as *Il17a*, *Il17f*, *Il17ra*, *Rorc*, and *Ccr6* (Fig. 5B), confirming that the reduced production of IL-17A protein in TLR2$^{-/-}$ Vγ6 γδ T cells is regulated at the transcriptional level. We also investigated the chromatin accessibility of *Il17a* loci in WT and TLR2$^{-/-}$ Vγ6 cells by ATAC-seq. Two open chromatin regions (OCRs) were called in *Il17a* loci of Vγ6 cells (Fig. 5C). Based on their genomic location and literature, we parsed one OCR in the promoter region of *Il17a* gene and the other OCR located at the conserved cis-regulatory element 2 (CNS2) region approximately 5500bp upstream of *Il17a* transcriptional start site (Akimzhanov et al., 2007; Wang et al., 2012). Comparing chromatin accessibility in *Il17a* loci of other IL-17A-producing cells, such as Vγ4 and ILC3 cells, as reported by ImmGen Consortium, we observed a prominent peak at the CNS2 region of their *Il17a* loci, confirming that this region serves as a conserved cis-regulatory element of *Il17a* loci in these IL-17A producing immune cells (Fig. S2B). Vγ6 cells from *C. mast*-

associated WT mice displayed significantly higher accessibility in *the Il17a* CNS2 region than those from *C. mast*-associated TLR2$^{-/-}$ mice (Fig. 5C). This finding corroborates that TLR2 signals regulate IL-17A production in Vγ6 cells at the transcriptomic and epigenomic levels.

To identify TLR2-mediated transcription factors (TFs) that influence accessibility of the *Il17a* CNS2 region, we screened TFs known to bind to the *Il17a* CNS2 region and compared their expression between WT and TLR2 deficient Vγ6 cells detected by RNAseq. Of particular interest to us was IκBζ (encoded by gene *nfkbiz)* because of its capacity to bind the *il17a* CNS2 locus in Th17 cells (Okamoto et al., 2010). Furthermore, its transcript levels correlated positively with TLR2 transcript expression quantified by RNAseq and real-time PCR (Fig. 5D).

To examine whether TLR2 activation increases the expression of IκBζ, which in turn promotes transcription of *Il17a*, we sorted Vγ6 cells from Vγ6 TCR-transgenic mice(Hayes et al., 2005), treated them with the TLR2 ligand Pam3CSK4 in vitro, and measured the gene expression of IκBζ and IL-17A. As expected, Vγ6 cells after Pam3CSK4 stimulation expressed more transcripts of both *nfkbiz* and *Il17a* compared to stimulation with IL-7 (Fig. 5E). Next, we generated IκBζ-deficient Vγ6 cells using a Cas9/gRNA ribonucleoprotein (RNP) transfection that targeted *nfkbiz* (Fig. S2C). Compared to Vγ6 cells transfected with a non-targeting control, IκBζ-deficient Vγ6 cells had diminished *Il17a* transcription (Fig. 5F). These findings indicate that TLR2 in Vγ6 cells promotes IL-17A production at the transcriptomic and epigenomic levels, at least in part through the involvement of IκBζ.

TLR2-deficient Vγ6 T cells show impaired fatty acid oxidation

Ingenuity Pathway Analysis (IPA) of differentially expressed genes in *C. mast*-associated mice revealed that WT Vγ6 T cells were enriched in the Oxidative Phosphorylation (OXPHOS) pathway (Fig. 6A). OXPHOS takes place in mitochondria and generates ATP through oxidation of nutrients to meet cellular energy demands. We assessed the mitochondrial mass in Vγ6 T cells using MitoTracker Green staining. Both WT and TLR2$^{-/-}$ Vγ6 cells displayed a similar increase in mitochondrial mass upon *C. mast* association, indicating TLR2 deficiency did not affect mitochondrial mass (Fig. S3A). The percentage of MitoSOX (mitochondria superoxide indicator)-positive cells was also comparable between TLR2$^{-/-}$ Vγ6 cells and WT Vγ6 cells (Fig. S3B). In contrast, MitoTracker™ Red CMXros staining, which measures mitochondrial membrane potential (ΔΨm), was reduced in *C. mast*-associated TLR2$^{-/-}$ Vγ6 cells (Fig. 6B), implying impaired mitochondrial activity. This was supported by a reduced ATP production in TLR2$^{-/-}$ Vγ6 cells compared to WT Vγ6 cells (Fig. 6C).

T Cells can generate ATP through the OXPHOS and/or glycolysis pathways. To determine which ATP production pathway is affected in TLR2$^{-/-}$ Vγ6 cells, we used metabolic flux analysis. To obtain sufficient TLR2$^{-/-}$ Vγ6 cells, we crossed Vγ6 TCR-transgenic mice (Hayes et al., 2005) onto a TLR2$^{-/-}$ background (denoted as WT Vγ6 Tg or TLR2$^{-/-}$ Vγ6 Tg, respectively). First, we wanted to verify that TLR2$^{-/-}$ Vγ6 Tg (double mutant) cells recapitulated the phenotype of Vγ6 cells from TLR2$^{-/-}$ mice with a conventional TCR repertoire. Stimulation with *C. mast* in the presence of WT DC confirmed that TLR2$^{-/-}$ Vγ6 Tg cells had similarly deficient IL-17A and ATP production to TLR2$^{-/-}$ Vγ6 cells from mice with a WT TCR repertoire (Fig. S3C). Next, we performed metabolic flux analysis comparing WT Vγ6 and TLR2$^{-/-}$ Vγ6 Tg cells using a Seahorse assay. The mitochondrial stress test revealed a significant decrease in basic and maximal oxygen consumption rate (OCR) in the TLR2$^{-/-}$ Vγ6 Tg cells compared to WT Vγ6 Tg cells (Fig. 6D-E). The cell-intrinsic role of TLR2 on OXPHOS was confirmed by direct Pam3CSK4 stimulation of Vγ6 cells *in vitro* (Fig. S3D). In contrast, the glycolytic proton efflux rate (glycoPER), which measures glycolysis, showed no differences between the two groups (Fig. S3E). Taken together, these findings indicated that, glycolysis was unaffected, but TLR2$^{-/-}$ Vγ6 cells exhibited impaired OXPHOS, leading to insufficient ATP production in these cells.

ATP production in mitochondria mainly comes from three substrates: glucose, long-chain fatty acid (LCFA), and glutamine. To determine the dominant substrate(s) in the energy metabolism of Vγ6 cells, we performed the Substrate Oxidation Stress Test on Vγ6 Tg cells from TLR2-sufficient Vγ6 Tg mice. Only etomoxir, an inhibitor of the LCFA oxidation pathway, significantly decreased both basic and maximal OCR in Vγ6 Tg cells (Fig. S3F), demonstrating that γδT17 cells utilize primarily fatty acid oxidation for energy production. To test whether TLR2 deficiency impairs the LCFA pathway in Vγ6 cells, we performed a Substrate Oxidation Stress Test on Vγ6 cells from WT Vγ6 Tg and TLR2$^{-/-}$ Vγ6 Tg mice inoculated with *C. mast*. Vγ6 cells from TLR2$^{-/-}$ Vγ6 Tg mice displayed a reduced basic and maximal OCR compared to WT Vγ6 Tg mice after etomoxir treatment, consistent with the reduced ATP content in TLR2$^{-/-}$ Vγ6 cells (Fig. 6 F-G). These data confirm that TLR2 signaling supports fatty acid oxidation (FAO) in Vγ6 cells.

Impaired Cpt1 function underlies the defective IL-17A response of TLR2-deficient Vγ6 cells

To further explore the underlying mechanisms, we studied the impact of TLR2 signaling on fatty acid oxidation (FAO) in Vγ6 γδ T cells. ATAC-seq data revealed that *C. mast* association activated an OCR within 2kb upstream of the *Cpt1a* gene, which encodes carnitine palmitoyl transferase 1a, a key enzyme involved in FAO (Fig. 7A). In addition, analysis of ImmGen Consortium data (Yoshida et al., 2019) identified the same OCR in the *Cpt1a* locus in IL-17A-producing ILC3s from small intestine, which harbors commensal microbiota (Fig. S4).

Notably, TLR2 deficiency decreased chromatin accessibility at *Cpt1a* (Fig. 7A). These data suggest that TLR2 signaling can enhance FAO by promoting the transcription of *Cpt1a,* which is also supported by our *in vitro* data showing that Pam3CSK4 stimulation upregulated *Cpt1a* in Vγ6 cells (Fig. 7B).

We next examined directly whether FAO is involved in TLR2-mediated IL-17 response in Vγ6 cells. Treatment with etomoxir, an irreversible inhibitor of *Cpt1a*, blocked the upregulation of *Il17a* induced by TLR2 activation (Fig. 7C). Notably, IκBζ, which in our hands upregulates *Il17a* in Vγ6 cells in response to TLR2 signaling, had also been reported to upregulate *Cpt1a* in fibroblastic reticular cells (Majumder et al., 2019). In line with this, IκBζ-deficient Vγ6 cells generated by Cas9/Crispr displayed reduced *Cpt1a* transcription (Fig. 7D). In the aggregate, our data support a sequence of events where, in response to endogenous TLR2 signaling in Vγ6 cells, increased expression of IκBζ enhances transcription of Cpt1a, thus favoring fatty acid oxidation and providing metabolic support for IL-17A production.

DISCUSSION

Our earlier studies demonstrated that the ocular commensal *C. mast* elicits expansion and IL-17A production by γδ T cells that provide local defense from pathogens at the ocular surface mucosal barrier. The current study explores mechanistically how these γδ T cells sense and respond to *C. mast*. We demonstrate that *C. mast* association activates TLR2 signals on both DCs and γδ T cells. While engagement of TLR2 on DC triggered the IL-1β essential to elicit γδ T cell IL-17 production, intrinsic TLR2 signaling in γδ T cells was also required. Our data reveal that intrinsic TLR2 signaling in γδ17 T cells acts in a subset-specific manner to enhance transcription of genes related to IL-17A production and activates the metabolic reprogramming to fatty acid oxidation that is needed to support IL-17A production.

Microorganisms activate TLR2 signaling in antigen-presenting cells and T cells (both αβ and γδ T cells) for IL-17A responses (Reynolds et al., 2010). In our investigation of *C. mast,* we were able to dissect the contribution of TLR2 expression in DCs from that of γδ T cells. Specifically, TLR2 activation in DCs by *C. mast* induced IL-1β, facilitating the proliferation and IL-17A production in γδ T cells. While both Vγ4 and Vγ6 cells exhibited IL-17A responses to *C. mast*, intrinsic TLR2 signals play a dominant role in Vγ6, but not Vγ4, cells for their proliferation and effector functions. The greater reliance on TLR2 signals for IL-17A responses in Vγ6 cells stimulated by *C. mast* are reminiscent of other reported phenotypes, e.g., in mouse gingiva, where the presence of Vγ6, but not Vγ4, cells is dependent on the presence of commensals

(O'Brien and Born, 2020; Wilharm et al., 2019). Based on our findings, we speculate that activation of innate receptors such as TLR2, by these commensals, may explain persistence in the gingival Vγ6, cells but not for Vγ4 cells. These phenotypes may perhaps be connected to the inherited innate-like behavior of Vγ6 cells towards *C. mast* and apparently also other commensals (Lu et al., 2015; Marchitto et al., 2019). Vγ4 cells, on the other hand, are later-stage responders, which may be explained by their need to receive TCR stimulation in addition to signals provided by DCs (St Leger et al., 2017).

TLR2 signals on Vγ6 cells target transcription factors in IL-17A regulation. We observed that TLR2 deficient Vγ6 cells displayed a decrease in the transcriptional expression of IκBζ. This transcription factor was found to upregulate *Il17a* in αβ Th17 cells (Okamoto et al., 2010). However, the need for IκBζ in IL-17A production by γδT17 cells has not been reported, and in view of the very different developmental and functional niches of these lineages, was not a given. In our hands, an *in vitro* knockout of IκBζ reduced *Il17a* transcript levels in Vγ6 cells, suggesting a supportive role of IκBζ in Vγ6 cells' IL-17A pathways. In addition to transcriptional regulation, we observed the epigenomic regulation mediated by TLR2 signaling at *Il17a* locus in Vγ6 cells, especially at the promoter and CNS2 region. The transcription factor IκBζ binds to the *Il17a* CNS2 region in αβ Th17 cells, facilitating IL-17 transcription (Okamoto et al., 2010). Although our study did not directly examine the binding of IκBζ to the *Il17a* regulatory region in Vγ6 cells, it stands to reason that lower binding of IκBζ to *Il17a* CNS2 region would contribute to the decreased *Il17a* transcripts in TLR2-deficienct Vγ6 cells. Notably, IκBζ does not act alone; it cooperates with Rorc to stimulate *Il17a* transcription in Th17 cells (Ciofani et al., 2012; Okamoto et al., 2010). Our RNA-sequencing data revealed a positive association between Rorc and TLR2 sufficiency, which supports the notion that Rorc upregulates Il17a through TLR2 signaling in Vγ6 cells. These findings suggest that TLR2 signaling utilizes multiple transcription factors that work together to regulate the transcriptional and epigenomic IL-17A program in Vγ6 cells.

Recent data made it clear that cell metabolism critically influences the functionality of immune cells. Cell metabolism is largely dictated by energy availability in the form of glucose, fatty acids, or other sources. However, other factors can impact cellular energy profiles. Here, we show that *C. mast*, through TLR2, can activate the OXPHOS pathway in γδ T cells, which then supports the production of IL-17A at the ocular surface. We posit that this finding parallels the situation found in the intestine, where colonizing segmented filamentous bacteria (SFB) can stimulate lipid metabolism in $CD4^+$ Th17 cells (Omenetti et al., 2019). Similarly, type 3 innate lymphoid cells (ILC3s) produce IL-17A in a manner that correlates with increased lipid metabolism (Di Luccia et al., 2019). These results, together with observations that germ-free

mice display impaired host metabolism and IL-17 responses at intestinal mucosal sites (Honda and Littman, 2016; Ivanov et al., 2009; Martin et al., 2009), suggest a shared metabolic regulation network across various mucosal surfaces that depends on the colonization of microbes at specific mucosal sites.

TLR2 signaling, functioning as a sensor of commensal bacteria, is involved in commensal-mediated metabolic adaptation in γδ T17 cells. While previous studies have reported the impact of TLR2 signals on proliferation, survival, and cytokine production in various T cell populations, our findings expand the understanding of TLR2 signaling in the metabolic regulation of γδT17 cells. TLR2-activated FAO can increase expression of the *Il17a* gene. Mechanistically, TLR2 signaling can upregulate the expression of *Cpt1a* in Vγ6 cells, which correlates with enhanced FAO capacity. Notably, IκBζ, which increases *Il17a* transcription, also enhances the expression of *Cpt1a* in Vγ6 cells. These data suggest a possible feed-forward mechanism where factors downstream of TLR2 signaling can epigenetically influence the future identity and metabolic profile of the cell. The mechanism(s) through which IkBζ promotes Cpt1a expression require(s) further investigation.

In summary, our results highlight the importance of intrinsic TLR2 signaling in γδ T cells to produce IL-17A in response to bacterial colonization. TLR2 signals enhance the expression of genes responsible for the IL-17A pathway and fatty acid metabolism in IL-17A-producing γδ T cells. Consequently, this study further links IL-17A production in γδ T cells with cell metabolism, implicating metabolic intervention as a potential strategy to modify γδ T cell functionality at mucosal and/or other barrier surfaces.

STAR METHODS

KEY RESOURCES TABLE

REAGENT or RESOURCE	SOURCE	IDENTIFIER
ANTIBODY		
FC: TLR2- PE (Clone: 6C2)	eBioscience	Cat#14-9021-82 (RRID: AB_468546)
FC: CD11b-BV421(Clone: M1/70)	BioLegend	Cat# 101235 (RRID: AB_10897942)
FC: CD11c- PerCP-Cy5.5 (Clone: N418)	BioLegend	Cat# 117328 (RRID: AB_2129641)
FC: TCRβ- FITC (H57-597)	eBioscience	Cat# 11-5961-82 (RRID: AB_465323)
FC: TCRγδ- APC (Clone: GL3)	eBioscience	Cat# 17-5711-82 (RRID: AB_842756)
FC: CD90.2- BV605 (Clone: 53-2.1)	BD	Cat# 536008 (RRID: AB_2665477)
FC: Vγ1- FITC (2.11)	BioLegend	Cat# 141104 (RRID: AB_10697031)
FC: Vγ4- PE-CY7(UC3-10A6)	eBioscience	Cat# 25-5828-82 (RRID: AB_2573474)
FC: 17D1	A gift from Robert Tigelaar	N/A
FC: Ly6G- APC-CY7(Clone:1A8)	BioLegend	Cat# 127624 (RRID: AB_10640819)
FC: IL-17A- BV650 (Clone: 17B7)	BD	Cat# 564170 (RRID: AB_2738641)
FC: CD69- BV785(Clone:H1.2F3)	BioLegend	Cat# 104543 (RRID: AB_2629640)
FC: Ki67- eFluor 506(Clone: SolA15)	eBioscience	Cat# 69-5698-82 (RRID: AB_2637482)
FC: ViaKrome 808 Fixable Viability Dye	Beckman Coulter	Cat# C36628
FC: CD45.1- FITC (clone:A20)	BioLegend	Cat# 110706 (RRID: AB_313494)
FC: CD45.2- AF700(clone:104)	eBioscience	Cat# 56-0454-82 (RRID: AB_657752)
FC: Annexin V- FITC	Invitrogen	Cat# A13199
FC: Phospho- S6 Ribosomal Protein(Ser235/236)-PE	Cell Signaling Technology	Cat# 5316S
In vitro: Anti-TCRγδ (Clone: UC7)	Bio X Cell	Cat# BE0070 (RRID: AB_1107751)
Chemical, Cytokine and Reagent		
CaCl2	Quality Biological	Cat# 351-130-721
Collagenase D	Roche	Cat# 45-11088866001
DNase I	Roche	Cat# 50-100-3290
Dispase II	Gibco	Cat# 17-105-041
Brefeldin A (Golgi-Plug)	BD PharMingen	Cat# 555029 (RRID: AB_2869014)
PMA/Ionomycin (Lymphocyte Activation Cocktail)	BD PharMingen	Cat# 550583 (RRID: AB_2868893)
Perm/Wash Buffer	BD Biosciences	Cat# 554723
BD PhosflowTM Fix Buffer I	BD Biosciences	Cat# 557870
BD PhosflowTM Perm Buffer III	BD Biosciences	Cat# 558050
Recombinant human IL-1beta	R&D system	Cat# 201-LB
CellEvent Caspase3/7 Green Detection Reagent	Invitrogen	Cat# C10423
TrizolTM Reagent	Invitrogen	Cat#15596026
MitroTracker Green FM	Invitrogen	Cat# M7514
MitoTracker Red CMXRos	Invitrogen	Cat# V35116B
MitoSOX Red mitochondrial Superoxide	Invitrogen	Cat# M36008
M-PER™ Mammalian Protein Extraction Reagent	Invitrogen	Cat# 78501
Poly-D-Lysine	Gibco	Cat# A3890401
Seahorse XF RPMI Medium	Agilent	Cat# 103576-100
Seahorse XF 1.0 M glucose solution	Agilent	Cat# 103577-100
Sodium Pyruvate (100 mM)	Gibco	Cat# 11360070
L-Glutamine (200 mM)	Gibco	Cat# A2916801
BODIPY™ FL C12	Invitrogen	Cat# C3927MP
BODIPY™ FL C16	Invitrogen	Cat# D3821
Pam3Cys-Ser-Lys4	Millipore	Cat# 506350
Adenosine 5′-triphosphate disodium salt hydrate	Sigma Aldrich	Cat# A7699
Critical Commercial Assays		
CD11c MicroBeads UltraPure, mouse	Miltenyi	Cat# 130-125-835
ELISA MAX™ Deluxe Set Mouse IL-17A	Biolegend	Cat# 432504
Mouse IL-1 beta/IL-1F2 DuoSet ELISA Kit	R&D	Cat# DY401
Mouse IL-23 DuoSet ELISA Kit	R&D	Cat# DY1887
miRNeasy Micro Kit	Qiagen	Cat# 217084

SMARTer® Ultra® Low Input RNA Kit for Sequencing - v3	Clontech	Cat# 634850
ATP Determination Kit	Invitrogen	Cat# A22066
Seahorse XFp Cell Mito Stress Test kit	Agilent	Cat# 103010
Seahorse XF Long Chain Fatty Acid Oxidation Stress Test Kit	Agilent	Cat#103672
Seahorse XF Glucose/Pyruvate Oxidation Stress Test Kit	Agilent	Cat#103673
Seahorse XF Glutamine Oxidation Stress Test Kit	Agilent	Cat# 103674
Seahorse XFp Glycolytic Rate Assay Kit	Agilent	Cat# 1033446
Oligonucleotides		
Nfkbiz_sgRNA1	IDT	Mm.Cas9.NFKBIZ.1.AA
Nfkbiz_sgRNA2	IDT	Mm.Cas9.NFKBIZ.1.AB
Nfkbiz_sgRNA1_T7 assay Forward: TGCGGTGATGTCTAGAAGGG	IDT	N/A
Nfkbiz_sgRNA1_T7 assay Reverse: GCTGACAGGTAAGAGCTCCA	IDT	N/A
Nfkbiz_sgRNA2_T7 assay Forward: TACTGAACCCACGGAATCCC	IDT	N/A
Nfkbiz_sgRNA2_T7 assay Rerverse: GCTGCTTGAGGGCTTTATCC	IDT	N/A
Control_sgRNA Alt-R CRISPR-Cas9 control Kit, 2 nmol	IDT	Cat#1072555
Software and algorithms		
FlowJo v10.4	Tree Star	https://www.flowjo.com
GraphPad Prism 9.1.1	GraphPad	https://www.graphpad.com

CONTACT FOR REAGENT AND RESOURCE SHARING

Further information and requests for resources and reagents should be directed to and will be fulfilled by the Lead Contact, Rachel Caspi (caspir@mail.nih.gov) and Xiaoyan Xu (xiaoyan.xu2@nih.gov

Data and Code availability

The RNA-seq datasets and the ATAC-seq datasets generated during this study are available at NCBI GEO (GSE236387). The code used for data analysis is shared at https://github.com/NIH-NEI/tlr2-ATAC-seq/

EXPERIMENTAL MODEL AND SUBJECT DETAILS

Mice

WT C57BL/6J mice were purchased from Jackson Laboratory. TLR2$^{-/-}$, TCRβ$^{-/-}$, and CD45.1 C57BL/6J mice originally from Jackson were bred and maintained in our animal facility. Vγ6 transgenic mice were generously provided by Paul E. Love; TLR2$^{-/-}$Vγ6 transgenic mice, and TLR2$^{-/-}$ TCRβ$^{-/-}$ mice were crossed and bred in house. For most in vivo and in vitro animal studies, male and female mice aged 6-10 weeks were used. All mice were housed under NIH SPF conditions. All mice received tear washes and were confirmed to lack ocular surface *C. mast* colonization before the experiment. All mouse studies were performed in full compliance with IACUC-approved protocols (NEI-690) and institutional guidelines.

Bacteria

C. mast was initially isolated from conjunctival homogenates that were plated on TSA + 5% blood agar plates kept at 37℃ in anaerobic conditions for 7 days. After original isolation, C. mast was propagated using TSA with 5% blood agar plates at 37℃ in an aerobic chamber (St Leger et al., 2017). Further, C. mast can be grown in blood heart infusion broth with 1% Tween 80 aerobically with shaking at 37℃.

METHOD DETAILS

C. mast Inoculation

C. mast was applied (10^8 CFU) to the ocular surface every three days for a total of three inoculations. Three weeks after the final inoculation, 10 µl PBS per eye was used to wash the conjunctiva to confirm colonization.

Tissue harvest and processing

Mice were euthanized by extensive cardiac perfusion. Two conjunctivae of one mouse were harvested by excising the eyelid and bulbar conjunctiva, combined, minced, and exposed to 0.9 ml of 1 mM $CaCl_2$, 2 mg/ml collagenase D, 0.16 mg/ml DNaseI and 0.05 mg/ml Dispase II in HBSS for 45 min at 37℃ with shaking. Cervical and submandibular lymph nodes were isolated, minced and exposed to 1mg/ml collagenase D for 30 min at 37℃ with shaking. After collagenase treatment, conjunctiva and draining lymph node cells were separately filtered through a 40 µm filter using a 1 cc syringe plunger. Then conjunctival cells were filtered a final time using a Corning Falcon Test Tube with Cell Strainer Snap Cap (Corning 352235).

CD11c Isolation

Mouse spleen tissue was cut into small pieces in RPMI medium containing 1mg/ml collagenase D. Tissue was incubated at 37°C and placed on a shaker for 1 hour. The single-cell suspension was prepared with a 70um filter and 1cc syringe plunger and was incubated with Miltenyi CD11c Isolation Beads and Fc Blocker for 10 mins on ice. CD11c positive selection was then performed following the manufacturer's protocol.

Cell sorting

Singe cell suspensions were prepared from cervical lymph nodes and spleen of WT or $TLR2^{-/-}$ mice. Total γδ T cell sorting: Fc blocker, APC anti-TCRγδ, and BV421 anti-TCRαβ antibody were added to the cell suspension in the FACS buffer and stained for 30 mins at room temperature. For Adoptive transfer: FITC anti- CD45.1, PE anti-TCRγδ, AF700 anti- CD45.2, BV510 anti-CD90.2 were mixed and stained. For RNA-seq cell sorting, FITC anti-Vγ1, PE-CY7 anti-Vγ4, APC anti-TCR γδ, and BV421-TCRαβ, BV510 anti-CD90.2 were mixed and stained cells for 30 mins. For ATAC-seq sorting, FITC anti-Vγ1, PE anti- TCRγδ, PE-CY7 anti-Vγ4, APC anti-CD62L, BV421-TCRαβ, BV510 anti-CD90.2 and BV785 anti- CD44 were mixed and added to cells. Propidium Iodide (PI) was added before each sorting, and cells were isolated by BD FACS Aria cell sorters.

Preparation for heat-killed *C. mast*

C. mast (1×10^6 CFU) was suspended in 100 µl PBS and heated at 60 °C for 30 mins.

In vitro γδ T cell and CD11c+ cell co-culture

$CD11c^+$ cells (1×10^5) were co-cultured with $TCR\gamma\delta^+$ cells (0.2×10^5) in 200 µl RPMI supplemented with 10% FBS for 72 hours under indicated conditions: 1 µl of heat-killed *C. mast* was added to 200 µl culture medium with 100 ng/mL IL-1β.

Flow Cytometry

In vitro assay: For intracellular staining, Brefeldin A (Golgi Plug) was added for the last 6 hours of 72-hour co-culture. After centrifugation, the supernatant was collected for ELISA assays. Cells were collected for flow cytometry. *In vivo* assay: tissue was homogenized in 2% FBS RPMI and filtered by a 40 µm strainer. The cells were stained following the manufacturer's protocol. For phospho-signal flow cytometry, we use BD Phosflow Fix Buffer and BD Phosflow Perm/Wash Buffer III. All the procedures followed by BD™ Phosflow Protocols for Mouse Splenocytes or Thymocytes. All samples were acquired with Beckman CytoFLEX LX Flow Cytometer and analyzed with FlowJo software.

ELISA

Cell supernatant was collected for IL-17A, IL1-β, IL-23 ELISA assays. Biolegend ELISA MAX™ Deluxe Set Mouse IL-17A (Cat# 432504), R&D Mouse IL-1 beta/IL-1F2 DuoSet ELISA (Cat# DY401), R&D Mouse IL-23 DuoSet ELISA Kit (Cat# DY1887) were used according to manufacturer's protocols.

Adoptive Transfer Assay

γδ T cells were sorted from CD45.1^{+} WT mice and CD45.2^{+} TLR2$^{-/-}$ mice (0.3 million cells each). Cells were mixed before being transferred to sublethal irradiated (450 rad) TCRγδ$^{-/-}$ mice.

RNA-seq

PI^{-}CD90.2^{+}TCRβ^{-}TCRγδ^{+}Vγ1^{+}Vγ4^{-} cells, PI^{-} CD90.2^{+}TCRβ^{-}TCRγδ^{+}Vγ1^{-}Vγ4^{+} cells, PI^{-} CD90.2^{+}TCRβ^{-}TCRγδ^{+}Vγ1^{-}Vγ4^{-}cells were sorted from naïve WT, naïve TLR2$^{-/-}$, *C. mast* inoculated WT and *C. mast* inoculated TLR2$^{-/-}$ mice. RNA was isolated using Qiagen miRNeasy Micro Kit. RNA was run on Agilent 2100 Bioanalyzer and RIN >8.0 was aimed to pass QC. RNA-seq was performed on Illumina Hiseq4000 (150pb, paired) using Clontech RNA Ultra Low Input Library Prep and paired-end sequencing in the NCI sequencing facility. Reads of the samples were trimmed for adapters and low-quality bases using Cutadapt before alignment with the reference genome (Mouse - mm10) and the annotated transcripts using STAR. The mapping statistics were calculated using Picard software. Library complexity is measured in terms of unique fragments in the mapped reads using Picard's MarkDuplicate utility. In addition, the gene expression quantification analysis was performed for all samples using STAR/RSEM tools.

ATAC-seq

DAPI^{-}CD90.2^{+}TCRβ^{-}TCRγδ^{+}Vγ1^{-}Vγ4^{-}CD27^{-}CD44^{hi} cells were sorted from naïve WT, naïve TLR2$^{-/-}$, *C. mast* inoculated WT, and *C. mast* inoculated TLR2$^{-/-}$ mice. Library preparation and sequencing were done by Novogene based on a previously reported method (Corces et al., 2017). Briefly, the nuclei extracted from the cells were quality controlled and suspended in the TruePrep Tagment Enzyme mix and incubated at 37°C for 30 min, followed by PCR amplification and purification with the AMPure beads. The quality-controlled library was quantified with Qubit 2.0, clustered using TruSeq PE Cluster Kit v3-cBot-HS (Illumina) and sequenced on an Illumina Hiseq platform to generate 150 bp paired-end reads. Raw data underwent rigorous quality control through FastqQC and FastP (Chen et al., 2018). Alignment was executed with Bowtie 2 (Langmead and Salzberg, 2012) and peaks were annotated using Genrich (Gaspar, 2021). ChiPseeker (Yu et al., 2015), and differential expression analysis relied on DESeq2 (Love et al., 2014). Homer2 was employed for motif analysis, and the UCSC genome browser (Karolchik et al., 2003) was the platform for peak visualization.

Extracellular flux analyses (Seahorse)

Experiments were performed on the Agilent Seahorse XF96 bioanalyzer. Freshly sorted γδ T cells were generated from *C. mast*$^{+}$ WT and TLR2 mice. γδ T cells were stimulated with PMA and Ionomycin for 3 hours before starting the Seahorse assay. Cells were washed with a prepared assay medium. Cells were plated onto XFp microplates (3×10^{5} cells/well) precoated with Poly-D Lysine (Thermo Fisher). The plates were centrifuged to immobilize cells. Cells were rested in assay medium in a non-CO2 incubator for 1hr prior to the assay. Oxidative phosphorylation-associated parameters were determined by Seahorse XFp Cell Mito Stress Test kit (Agilent, #103010) with three injections: (1) 2.5 μM oligomycin, (2) 2.5 μM FCCP, and (3) 1 μM rotenone/antimycin A. For the XF Substrate Oxidation Stress Test kit (Agilent, #103672, #103673, #103674), Oxidative phosphorylation associated parameters were determined with four injections: (1) 2.5 μM oligomycin, (2) 4.0 μM Etomoxir/ 2.0 μM UK5099/ 3.0μM BPTES (3) 2.5 μM FCCP, and (4) 1 μM rotenone/antimycin A. Glycolysis associated parameters were determined by Seahorse XFp Glycolytic Rate Assay Kit (Agilent #1033446) with two injections: (1) 0.5 μM rotenone/ antimycin A; (2) 50 mM 2-DG.

Mitochondrial ROS measurement

Cells were collected from PBS-treated and *C. mast*-treated WT and TLR2$^{-/-}$ mice. Cells were incubated with a MitoSOX probe (Invitrogen, Cat. # M36008) for 10 min at 37℃. After incubation, cells were washed and stained for other surface markers. Then cells were subjected to flow cytometry analysis.

ATP level determination

γδ T cells were sorted from *C. mast* inoculated WT and TLR2$^{-/-}$ Vg6 transgenic mice and placed in 96 well, pre-coated with anti-TCRγδ (2μg/ml) the previous night. Cells were harvested 3 days post in vitro activation, washed with RPMI-1640 medium three times, and counted. Cells were rested in 96-well for 3 hours at 37℃. Cells were quickly spun down and lysed in a native lysis buffer (Cell Signaling Technology) for 10 min on ice. Cells were then centrifuged at 2000 g for 10 min and the supernatants were collected. ATP levels were measured according to the manufacturer's instructions (Invitrogen, #A22066).

CRISPR mutation of IκBζ in Vγ6 cells

To mutate IκBζ in Vγ6 cells, CRISPR-Cas9 ribonucleoprotein (RNP) complexes were delivered into Vγ6 Tg cells using electroporation with the Amaxa Nucleofector system (Lonza). RNP complexes are made up of 150 pmol sgRNA, 10 ug Cas9 nuclease and 20 mM Alt-R Cas9 Electroporation Enhancer (Integrated DNA Technologies, Inc) as described previously (Soyoung A. Oh et al., 2019). sgRNAs were designed using the Crispr guide design software (Integrated DNA Technologies, Inc).

QUANTITATION AND STATISTICAL ANALYSIS

GraphPad Prism 9.1.1 were used for statistical analyses. Welch's t-test, Mann-Whitney U test, or Wilson t-test was used as indicated in the figure and/ or legends. N values, replicate experiments are all located in figure legends. *P<0.05, **P<0.01, ***P <0.001.

ACKNOWLEDGMENTS

This work was supported by the intramural Research Program of the NIH, National Eye Institute (project EY000184; R.R. Caspi). The authors thank the staff of the NEI and the NHLBI Flow Cytometry Core Facilities for excellent sorting and analysis, and the NCI sequencing facility and Novogene for sequencing services. We gratefully acknowledge the editorial assistance of the NIH Fellows Editorial Board.

REFERENCES

Acosta-Rodriguez, E.V., L. Rivino, J. Geginat, D. Jarrossay, M. Gattorno, A. Lanzavecchia, F. Sallusto, and G. Napolitani. 2007. Surface phenotype and antigenic specificity of human interleukin 17–producing T helper memory cells. *Nature Immunology* 8:639-646.

Akimzhanov, A.M., X.O. Yang, and C. Dong. 2007. Chromatin remodeling of interleukin-17 (IL-17)-IL-17F cytokine gene locus during inflammatory helper T cell differentiation. *J Biol Chem* 282:5969-5972.

Akira, S., and K. Takeda. 2004. Toll-like receptor signalling. *Nat Rev Immunol* 4:499-511.

Cai, Y., F. Xue, H. Qin, X. Chen, N. Liu, C. Fleming, X. Hu, H.G. Zhang, F. Chen, J. Zheng, and J. Yan. 2019. Differential Roles of the mTOR-STAT3 Signaling in Dermal gammadelta T Cell Effector Function in Skin Inflammation. *Cell Rep* 27:3034-3048 e3035.

Chen, S., Y. Zhou, Y. Chen, and J. Gu. 2018. fastp: an ultra-fast all-in-one FASTQ preprocessor. *Bioinformatics* 34:i884-i890.

Ciofani, M., A. Madar, C. Galan, M. Sellars, K. Mace, F. Pauli, A. Agarwal, W. Huang, C.N. Parkhurst, M. Muratet, K.M. Newberry, S. Meadows, A. Greenfield, Y. Yang, P. Jain, F.K. Kirigin, C. Birchmeier, E.F. Wagner, K.M. Murphy, R.M. Myers, R. Bonneau, and D.R. Littman. 2012. A validated regulatory network for Th17 cell specification. *Cell* 151:289-303.

Conti, H.R., A.C. Peterson, L. Brane, A.R. Huppler, N. Hernández-Santos, N. Whibley, A.V. Garg, M.R. Simpson-Abelson, G.A. Gibson, A.J. Mamo, L.C. Osborne, S. Bishu, N. Ghilardi, U. Siebenlist, S.C. Watkins, D. Artis, M.J. McGeachy, and S.L. Gaffen. 2014. Oral-resident natural Th17 cells and γδ T cells control opportunistic Candida albicans infections. *J Exp Med* 211:2075-2084.

Corces, M.R., A.E. Trevino, E.G. Hamilton, P.G. Greenside, N.A. Sinnott-Armstrong, S. Vesuna, A.T. Satpathy, A.J. Rubin, K.S. Montine, B. Wu, A. Kathiria, S.W. Cho, M.R. Mumbach, A.C. Carter, M. Kasowski, L.A. Orloff, V.I. Risca, A. Kundaje, P.A. Khavari, T.J. Montine, W.J. Greenleaf, and H.Y. Chang. 2017. An improved ATAC-seq protocol reduces background and enables interrogation of frozen tissues. *Nat Methods* 14:959-962.

de Paiva, C.S., A.J. St Leger, and R.R. Caspi. 2022. Mucosal immunology of the ocular surface. *Mucosal Immunol* 15:1143-1157.

Di Luccia, B., S. Gilfillan, M. Cella, M. Colonna, and S.C. Huang. 2019. ILC3s integrate glycolysis and mitochondrial production of reactive oxygen species to fulfill activation demands. *J Exp Med* 216:2231-2241.

Duan, J., H. Chung, E. Troy, and D.L. Kasper. 2010. Microbial colonization drives expansion of IL-1 receptor 1-expressing and IL-17-producing gamma/delta T cells. *Cell host & microbe* 7:140-150.

Edwards, S.C., C.E. Sutton, K. Ladell, E.J. Grant, J.E. McLaren, F. Roche, P. Dash, N. Apiwattanakul, W. Awad, K.L. Miners, S.J. Lalor, J.C. Ribot, S. Baik, B. Moran, A. McGinley, V. Pivorunas, L. Dowding, M. Macoritto, J. Paez-Cortez, A. Slavin, G. Anderson, B. Silva-Santos, K. Hokamp, D.A. Price, P.G. Thomas, R.M. McLoughlin, and K.H.G. Mills. 2020. A population of proinflammatory T cells coexpresses αβ and γδ T cell receptors in mice and humans. *J Exp Med* 217:

Gadjeva, M., J. Nagashima, T. Zaidi, R.A. Mitchell, and G.B. Pier. 2010. Inhibition of macrophage migration inhibitory factor ameliorates ocular Pseudomonas aeruginosa-induced keratitis. *PLoS Pathog* 6:e1000826.

Gaspar, J.M. 2021. Genrich: detecting sites of genomic enrichment. In.

Gomez-Rodriguez, J., E.A. Wohlfert, R. Handon, F. Meylan, J.Z. Wu, S.M. Anderson, M.R. Kirby, Y. Belkaid, and P.L. Schwartzberg. 2014. Itk-mediated integration of T cell receptor and cytokine signaling regulates the balance between Th17 and regulatory T cells. *Journal of Experimental Medicine* 211:529-543.

Hayes, S.M., L. Li, and P.E. Love. 2005. TCR Signal Strength Influences αβ/γδ Lineage Fate. *Immunity* 22:583-593.

Heilig, J.S., and S. Tonegawa. 1986. Diversity of murine gamma genes and expression in fetal and adult T lymphocytes. *Nature* 322:836-840.

Honda, K., and D.R. Littman. 2016. The microbiota in adaptive immune homeostasis and disease. *Nature* 535:75-84.

Ivanov, II, K. Atarashi, N. Manel, E.L. Brodie, T. Shima, U. Karaoz, D. Wei, K.C. Goldfarb, C.A. Santee, S.V. Lynch, T. Tanoue, A. Imaoka, K. Itoh, K. Takeda, Y. Umesaki, K. Honda, and D.R. Littman. 2009. Induction of intestinal Th17 cells by segmented filamentous bacteria. *Cell* 139:485-498.

Karolchik, D., R. Baertsch, M. Diekhans, T.S. Furey, A. Hinrichs, Y.T. Lu, K.M. Roskin, M. Schwartz, C.W. Sugnet, D.J. Thomas, R.J. Weber, D. Haussler, and W.J. Kent. 2003. The UCSC Genome Browser Database. *Nucleic Acids Res* 31:51-54.

Knop, E., and N. Knop. 2005. The role of eye-associated lymphoid tissue in corneal immune protection. *J Anat* 206:271-285.

Langmead, B., and S.L. Salzberg. 2012. Fast gapped-read alignment with Bowtie 2. *Nat Methods* 9:357-359.

Li, X., R. Bechara, J. Zhao, M.J. McGeachy, and S.L. Gaffen. 2019. IL-17 receptor–based signaling and implications for disease. *Nature Immunology* 20:1594-1602.

Lopes, N., C. McIntyre, S. Martin, M. Raverdeau, N. Sumaria, A.C. Kohlgruber, G.J. Fiala, L.Z. Agudelo, L. Dyck, H. Kane, A. Douglas, S. Cunningham, H. Prendeville, R. Loftus, C. Carmody, P. Pierre, M. Kellis, M. Brenner, R.J. Arguello, B. Silva-Santos, D.J. Pennington, and L. Lynch. 2021. Distinct metabolic programs established in the thymus control effector functions of gammadelta T cell subsets in tumor microenvironments. *Nat Immunol* 22:179-192.

Love, M.I., W. Huber, and S. Anders. 2014. Moderated estimation of fold change and dispersion for RNA-seq data with DESeq2. *Genome Biol* 15:550.

Lu, Y., X. Cao, X. Zhang, and D. Kovalovsky. 2015. PLZF Controls the Development of Fetal-Derived IL-17+Vgamma6+ gammadelta T Cells. *J Immunol* 195:4273-4281.

Majumder, S., N. Amatya, S. Revu, C.V. Jawale, D. Wu, N. Rittenhouse, A. Menk, S. Kupul, F. Du, I. Raphael, A. Bhattacharjee, U. Siebenlist, T.W. Hand, G.M. Delgoffe, A.C. Poholek, S.L. Gaffen, P.S. Biswas, and M.J. McGeachy. 2019. IL-17 metabolically reprograms activated fibroblastic reticular cells for proliferation and survival. *Nat Immunol* 20:534-545.

Marchitto, M.C., C.A. Dillen, H. Liu, R.J. Miller, N.K. Archer, R.V. Ortines, M.P. Alphonse, A.I. Marusina, A.A. Merleev, Y. Wang, B.L. Pinsker, A.S. Byrd, I.D. Brown, A. Ravipati, E. Zhang, S.S. Cai, N. Limjunyawong, X. Dong, M.R. Yeaman, S.I. Simon, W. Shen, S.K. Durum, R.L. O'Brien, E. Maverakis, and L.S. Miller. 2019. Clonal Vγ6(+)Vδ4(+) T cells promote IL-17-mediated immunity against Staphylococcus aureus skin infection. *Proceedings of the National Academy of Sciences of the United States of America* 116:10917-10926.

Marks, K.E., S. Flaherty, K.M. Patterson, M. Stratton, G.J. Martinez, and J.M. Reynolds. 2021. Toll-like receptor 2 induces pathogenicity in Th17 cells and reveals a role for IPCEF in regulating Th17 cell migration. *Cell Rep* 35:109303.

Martin, B., K. Hirota, D.J. Cua, B. Stockinger, and M. Veldhoen. 2009. Interleukin-17-producing gammadelta T cells selectively expand in response to pathogen products and environmental signals. *Immunity* 31:321-330.

Mokuno, Y., T. Matsuguchi, M. Takano, H. Nishimura, J. Washizu, T. Ogawa, O. Takeuchi, S. Akira, Y. Nimura, and Y. Yoshikai. 2000. Expression of toll-like receptor 2 on gamma delta T cells bearing invariant V gamma 6/V delta 1 induced by Escherichia coli infection in mice. *J Immunol* 165:931-940.

O'Brien, R.L., and W.K. Born. 2020. Two functionally distinct subsets of IL-17 producing γδ T cells. *Immunol Rev* 298:10-24.

Okamoto, K., Y. Iwai, M. Oh-Hora, M. Yamamoto, T. Morio, K. Aoki, K. Ohya, A.M. Jetten, S. Akira, T. Muta, and H. Takayanagi. 2010. IkappaBzeta regulates T(H)17 development by cooperating with ROR nuclear receptors. *Nature* 464:1381-1385.

Oliveira-Nascimento, L., P. Massari, and L.M. Wetzler. 2012. The Role of TLR2 in Infection and Immunity. *Front Immunol* 3:79.

Omenetti, S., C. Bussi, A. Metidji, A. Iseppon, S. Lee, M. Tolaini, Y. Li, G. Kelly, P. Chakravarty, S. Shoaie, M.G. Gutierrez, and B. Stockinger. 2019. The Intestine Harbors Functionally Distinct Homeostatic Tissue-Resident and Inflammatory Th17 Cells. *Immunity* 51:77-89.e76.

Reynolds, J.M., B.P. Pappu, J. Peng, G.J. Martinez, Y. Zhang, Y. Chung, L. Ma, X.O. Yang, R.I. Nurieva, Q. Tian, and C. Dong. 2010. Toll-like receptor 2 signaling in CD4(+) T lymphocytes promotes T helper 17 responses and regulates the pathogenesis of autoimmune disease. *Immunity* 32:692-702.

Roark, C.L., M.K. Aydintug, J. Lewis, X. Yin, M. Lahn, Y.S. Hahn, W.K. Born, R.E. Tigelaar, and R.L. O'Brien. 2004. Subset-specific, uniform activation among V gamma 6/V delta 1+ gamma delta T cells elicited by inflammation. *J Leukoc Biol* 75:68-75.

Sherlock, J.P., B. Joyce-Shaikh, S.P. Turner, C.C. Chao, M. Sathe, J. Grein, D.M. Gorman, E.P. Bowman, T.K. McClanahan, J.H. Yearley, G. Eberl, C.D. Buckley, R.A. Kastelein, R.H. Pierce, D.M. Laface, and D.J. Cua. 2012. IL-23 induces spondyloarthropathy by acting on ROR-γt+ CD3+CD4-CD8- entheseal resident T cells. *Nat Med* 18:1069-1076.

Shibata, K., H. Yamada, H. Hara, K. Kishihara, and Y. Yoshikai. 2007. Resident Vdelta1+ gammadelta T cells control early infiltration of neutrophils after Escherichia coli infection via IL-17 production. *J Immunol* 178:4466-4472.

St Leger, A.J., J.V. Desai, R.A. Drummond, A. Kugadas, F. Almaghrabi, P. Silver, K. Raychaudhuri, M. Gadjeva, Y. Iwakura, M.S. Lionakis, and R.R. Caspi. 2017. An Ocular Commensal Protects against Corneal Infection by Driving an Interleukin-17 Response from Mucosal gammadelta T Cells. *Immunity* 47:148-158 e145.

St Leger, A.J., A.M. Hansen, H. Karauzum, R. Horai, C.R. Yu, A. Laurence, K.D. Mayer-Barber, P. Silver, R. Villasmil, C. Egwuagu, S.K. Datta, and R.R. Caspi. 2018. STAT-3-independent production of IL-17 by mouse innate-like alphabeta T cells controls ocular infection. *J Exp Med* 215:1079-1090.

Suryawanshi, A., T. Veiga-Parga, N.K. Rajasagi, P.B. Reddy, S. Sehrawat, S. Sharma, and B.T. Rouse. 2011. Role of IL-17 and Th17 cells in herpes simplex virus-induced corneal immunopathology. *J Immunol* 187:1919-1930.

Sutton, C.E., S.J. Lalor, C.M. Sweeney, C.F. Brereton, E.C. Lavelle, and K.H. Mills. 2009. Interleukin-1 and IL-23 induce innate IL-17 production from gammadelta T cells, amplifying Th17 responses and autoimmunity. *Immunity* 31:331-341.

Wang, X., Y. Zhang, X.O. Yang, R.I. Nurieva, S.H. Chang, S.S. Ojeda, H.S. Kang, K.S. Schluns, J. Gui, A.M. Jetten, and C. Dong. 2012. Transcription of Il17 and Il17f is controlled by conserved noncoding sequence 2. *Immunity* 36:23-31.

Wilharm, A., Y. Tabib, M. Nassar, A. Reinhardt, G. Mizraji, I. Sandrock, O. Heyman, J. Barros-Martins, Y. Aizenbud, A. Khalaileh, L. Eli-Berchoer, E. Elinav, A. Wilensky, R. Forster, H. Bercovier, I. Prinz, and A.H. Hovav. 2019. Mutual interplay between IL-17-producing gammadeltaT cells and microbiota orchestrates oral mucosal homeostasis. *Proceedings of the National Academy of Sciences of the United States of America* 116:2652-2661.

Yoshida, H., C.A. Lareau, R.N. Ramirez, S.A. Rose, B. Maier, A. Wroblewska, F. Desland, A. Chudnovskiy, A. Mortha, C. Dominguez, J. Tellier, E. Kim, D. Dwyer, S. Shinton, T. Nabekura, Y. Qi, B. Yu, M. Robinette, K.W. Kim, A. Wagers, A. Rhoads, S.L. Nutt, B.D. Brown, S. Mostafavi, J.D. Buenrostro, and C. Benoist. 2019. The cis-Regulatory Atlas of the Mouse Immune System. *Cell* 176:897-912.e820.

Yu, G., L.G. Wang, and Q.Y. He. 2015. ChIPseeker: an R/Bioconductor package for ChIP peak annotation, comparison and visualization. *Bioinformatics* 31:2382-2383.

Zhou, L., Ivanov, II, R. Spolski, R. Min, K. Shenderov, T. Egawa, D.E. Levy, W.J. Leonard, and D.R. Littman. 2007. IL-6 programs T(H)-17 cell differentiation by promoting sequential engagement of the IL-21 and IL-23 pathways. *Nat Immunol* 8:967-974.

Figures

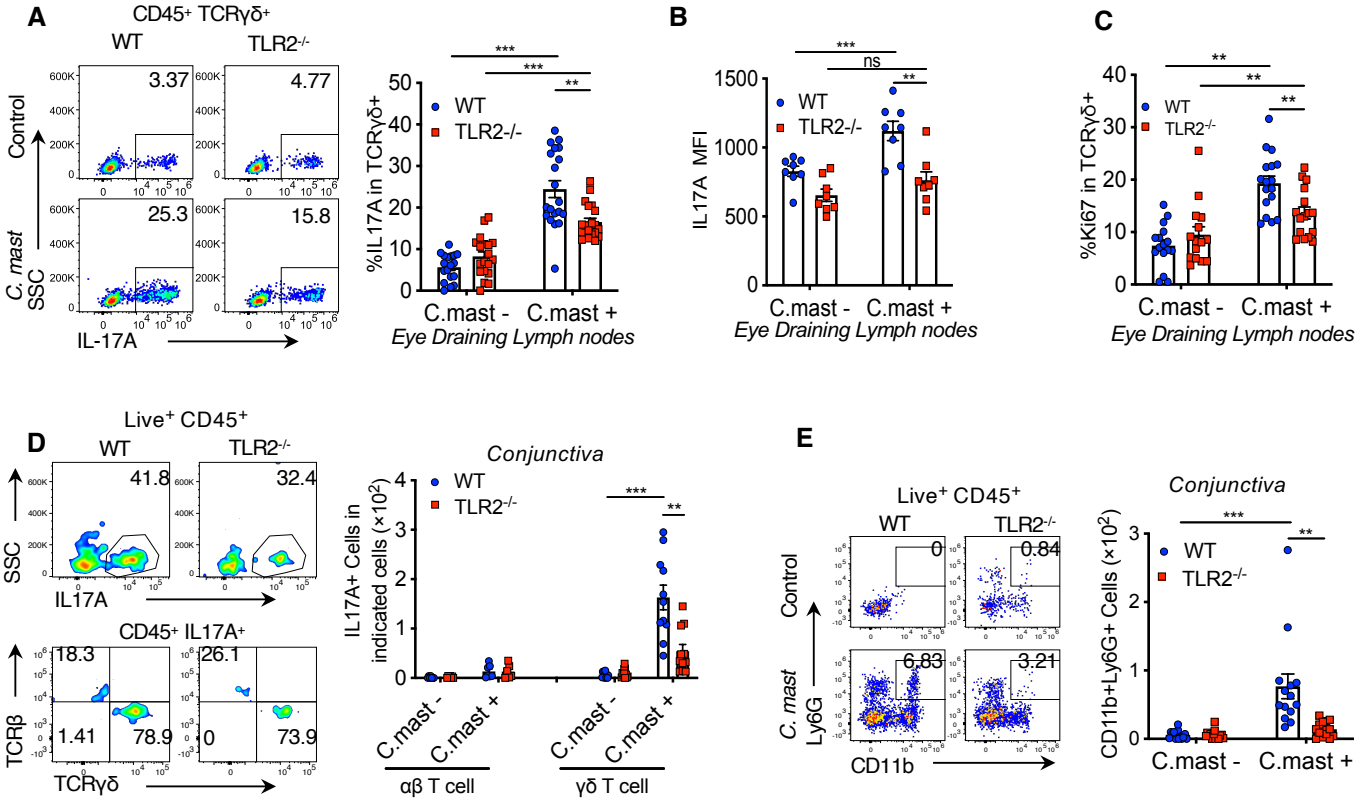

Figure 1. TLR2 is required for IL-17A production in response to *C. mast* at the ocular surface

C. mast (10^8 CFU) or PBS was instilled onto each eye every 3 days for a total of 3 treatments.
(A) Representative FACS plots and bar graphs showing the percentage of IL17A$^+$ in γδ T cells from eye-draining lymph nodes. N= 20. Combined data from 6 experiments.
(B) Bars depict geometric mean fluorescence intensity (MFI) of IL17A in eye-draining lymph node γδ T cells. N= 8. Combined data from 2 experiments
(C) The percentage of Ki67+ γδ T cells in eye draining lymph node. N=15-17. Combined data from 5-6 experiments.
(D) Representative FACS plots showing the percentage of IL-17A-producing cells (top panels), IL17A+TCRαβ+ cells, and IL-17A+TCRγδ+ cells in the conjunctiva (bottom panels). Bar graphs show the number of conjunctival IL17A+TCRαβ+ cells and IL-17A+TCRγδ+ cells. IL17A+TCRαβ+ cells: data combined from 2 experiments. N= 7. IL-17A+TCRγδ+ cells: data combined from 5 experiments. N=14 per group.
(E) Representative FACS plots and bar graphs showing the cell number of conjunctival neutrophils in WT and TLR2$^{-/-}$ mice with/without *C. mast* inoculation. N=14. Combined data from 5 experiments.
(A-F) Bars represent mean ± SEM with *P<0.05, **P<0.01, ***P <0.001. Statistical significance was determined by Welch's t-test (A-B, D) or Mann-Whithney test (C, E).

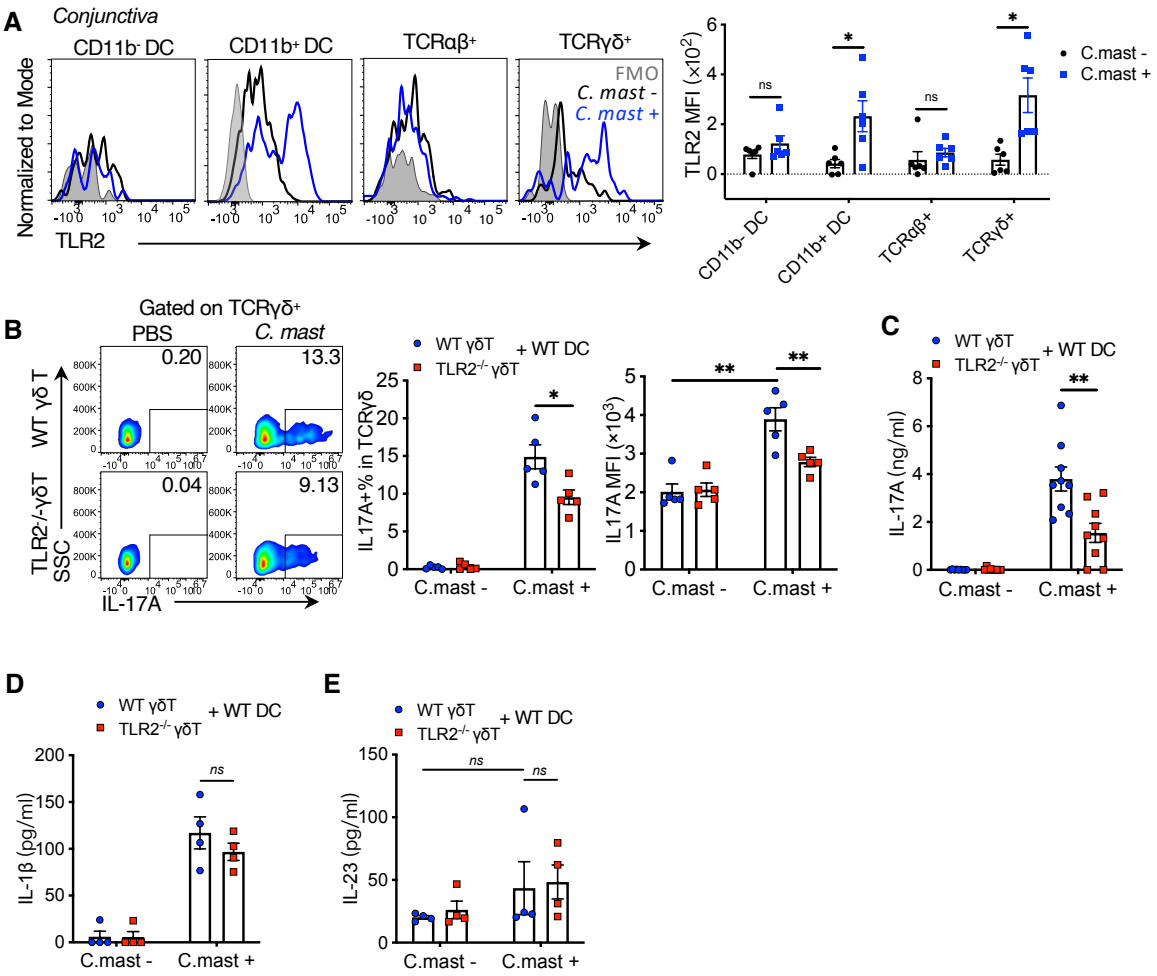

Figure 2. TLR2 expression in γδ T cells is needed for full IL-17A Responses to *C. mast*

WT or TLR2$^{-/-}$ γδ T cells were sorted by flow cytometry from naive mice and co-cocultured with WT CD11c^{+} dendritic cells for 72 hours (γδ T cells: 2×10^{4}; CD11c+ cells: 1×10^{5}) with/ without heat-killed *C. mast*. Supernatants and cells were collected for ELISA or flow cytometry analysis.

(A) Representative FACS plots and bar graphs depicting TLR2 expression in CD11b^{-} DC, CD11b^{+} DC, TCRαβ^{+} and TCRγδ^{+} cells in the conjunctiva of C57BL/6J WT mice with or without *C. mast* association. N = 5 per group. Combined data from 2 experiments.

(B) Representative FACS plots and bar plots showing the percentage and MFI of IL-17A on γδ T cells from WT or TLR2$^{-/-}$ γδ T cell co-culture system. N= 5. Combined data from 3 experiments.

(C-E) Bar graphs presenting the levels of IL-17A **(C),** IL-1β **(D)**, and IL-23 **(E)** in the supernatants from WT or TLR2$^{-/-}$ γδ T cell co-culture system. Data was combined from 4 experiments (N= 9) for (C); and 2 experiments (N= 4) for (D-E).

(A-E) Bars represent mean ± SEM with *P<0.05, **P<0.01, ***P <0.001. Statistical significance was determined by Welch's t-test.

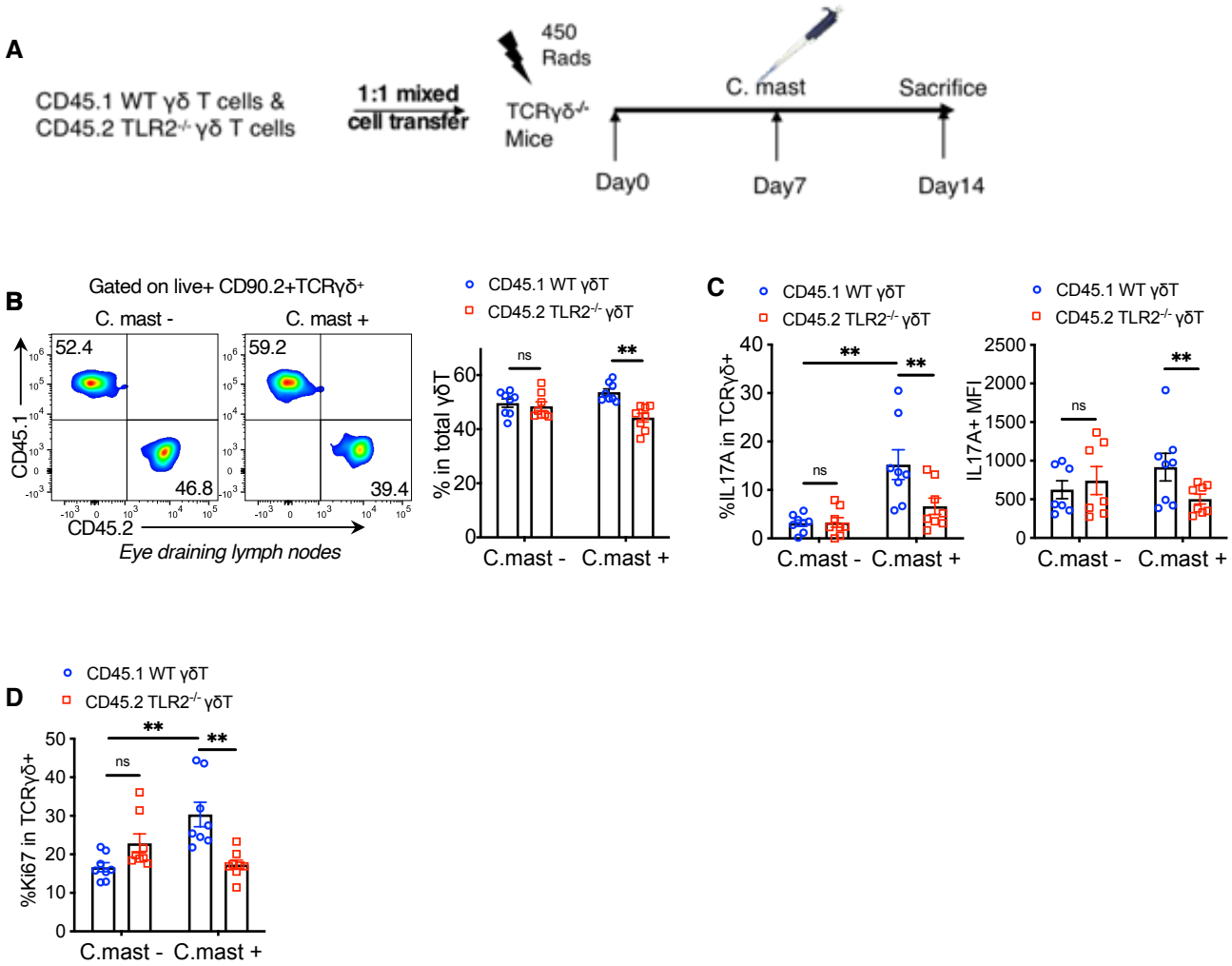

Figure 3. TLR2 deficiency in γδ T cells blunts IL-17A and proliferative responses *in vivo*

A 1:1 mix of CD45 allotype-marked WT and TLR2$^{-/-}$ γδ T cells was infused into TCRδ$^{-/-}$ mice. Cells were collected after 2 weeks for *ex vivo* analysis after PMA/Ionomycin stimulation.
(A) Schematic representation of the γδ T cell adoptive transfer experiment.
(B) Representative FACS plots and bar plots showing the ratio of CD45.1^{+} WT γδ T cells and CD45.2^{+} TLR2$^{-/-}$ γδ T cells in the eye-draining lymph nodes from host mice 2 weeks after adoptive transfer with/without *C. mast* inoculation. N= 8.
(C) The percentage of IL-17A+ cells and IL-17A expression (MFI) of WT and TLR2$^{-/-}$ γδ T cells in the eye-draining lymph nodes from host mice after adoptive transfer with/without *C. mast* inoculation. N= 8.
(D) The percentage of Ki67+ cells from WT and TLR2$^{-/-}$ γδ T cells from host mice with/without *C. mast* inoculation. (B-D) N=8. Data were combined from 4 experiments.
Bars represent mean ± SEM with *P<0.05, **P<0.01, ***P <0.001. Statistical significance was determined by the Wilcoxon signed-rank test.

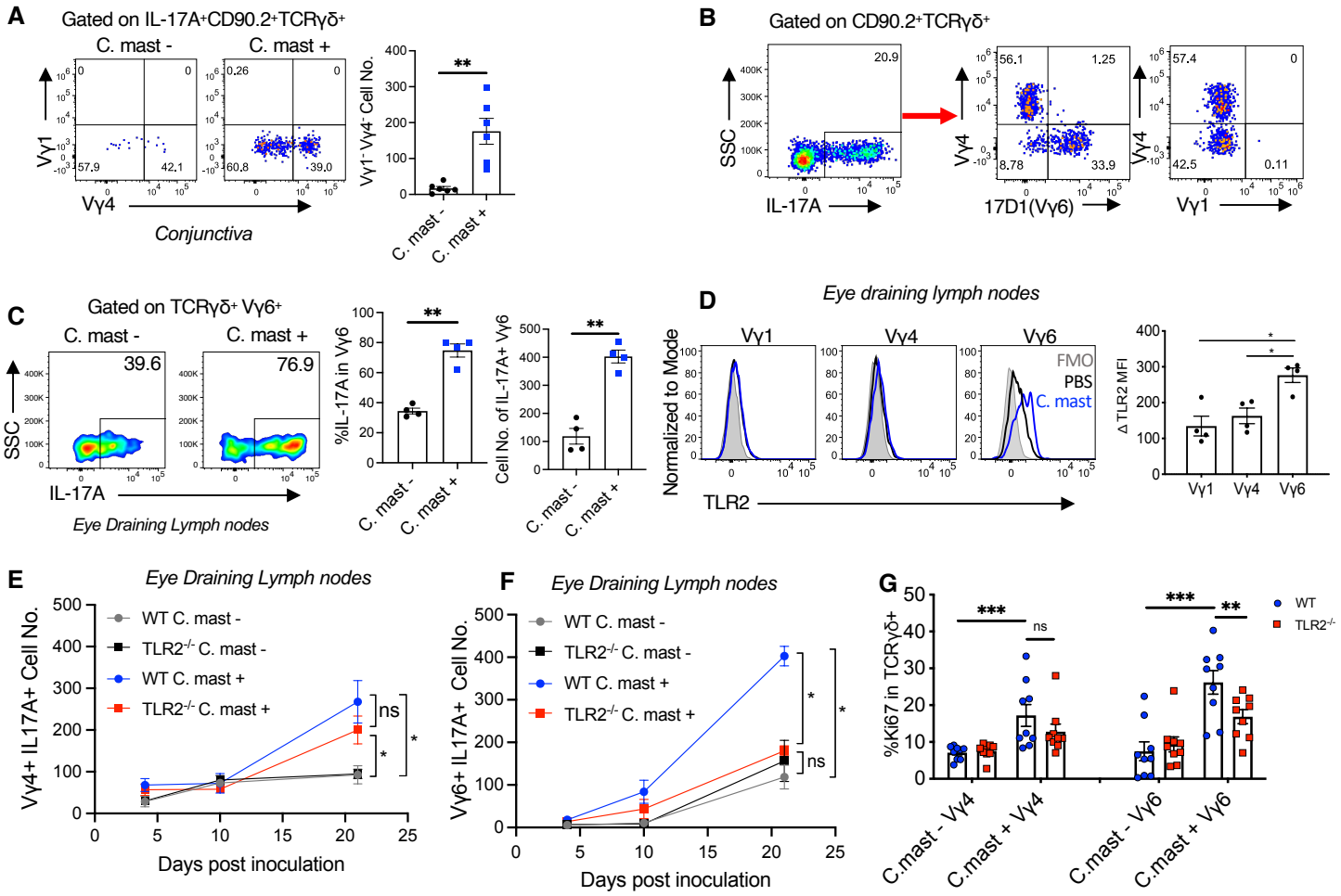

Figure 4. TLR2$^{-/-}$ Vγ6 cells exhibit a more profoundly impaired response to *C. mast than* Vγ4 cells

C. mast (CFU =10^8) or PBS was instilled into each eye of C57BL/6J wild-type mice every 3 days for a total of 3 times. **(A-D).**

(**A**)Representative FACS plots and bar graphs representing the number of IL-17A$^+$ Vγ1$^-$Vγ4$^-$ γδ T in the conjunctiva of wild-type mice with/without *C. mast* inoculation. N= 6. Data were combined from 2 experiments.

(B) Representative FACS plots showing the percentage of Vγ1$^+$, Vγ4$^+$, and Vγ6$^+$ cells among IL-17A producing γδ T cells of eye-draining lymph nodes with or without *C. mast* inoculation. N= 3.

(C) The percentage and the number of IL-17$^+$ Vγ6 cells in eye-draining lymph nodes with or without *C. mast* inoculation. N= 4.

(D) Representative FACS plots representing TLR2 expression in the indicated γδ T cell subset and bar graphs depicting normalized TLR2 mean fluorescein intensity (denoted as Δ MFI) of the indicated γδ subsets in eye draining lymph nodes. N=4. (Δ MFI = averaged MFI of TLR2 in *C. mast*$^+$ group – Averaged MFI of TLR2 in *C. mast*$^-$ group)

(E-F) Kinetic experiment showing cell numbers of IL17A$^+$ Vγ4$^+$ **(E)** and IL17A$^+$ Vγ6$^+$ **(F)** from WT and TLR2$^{-/-}$ mice with or without *C. mast* inoculation on the indicated days. N = 4.

(G) Bar plot showing Ki-67 expression of γδ T cells in Vγ4 and Vγ6 subsets in WT and TLR2$^{-/-}$ mice with/without *C. mast* inoculation. N=17. Combined data from 3 experiments.

Bars represent mean ± SEM with *P<0.05, **P<0.01, ***P <0.001. Statistical significance was determined by Welch's t-test (D-F) or Whitney U test (A, B, C, G).

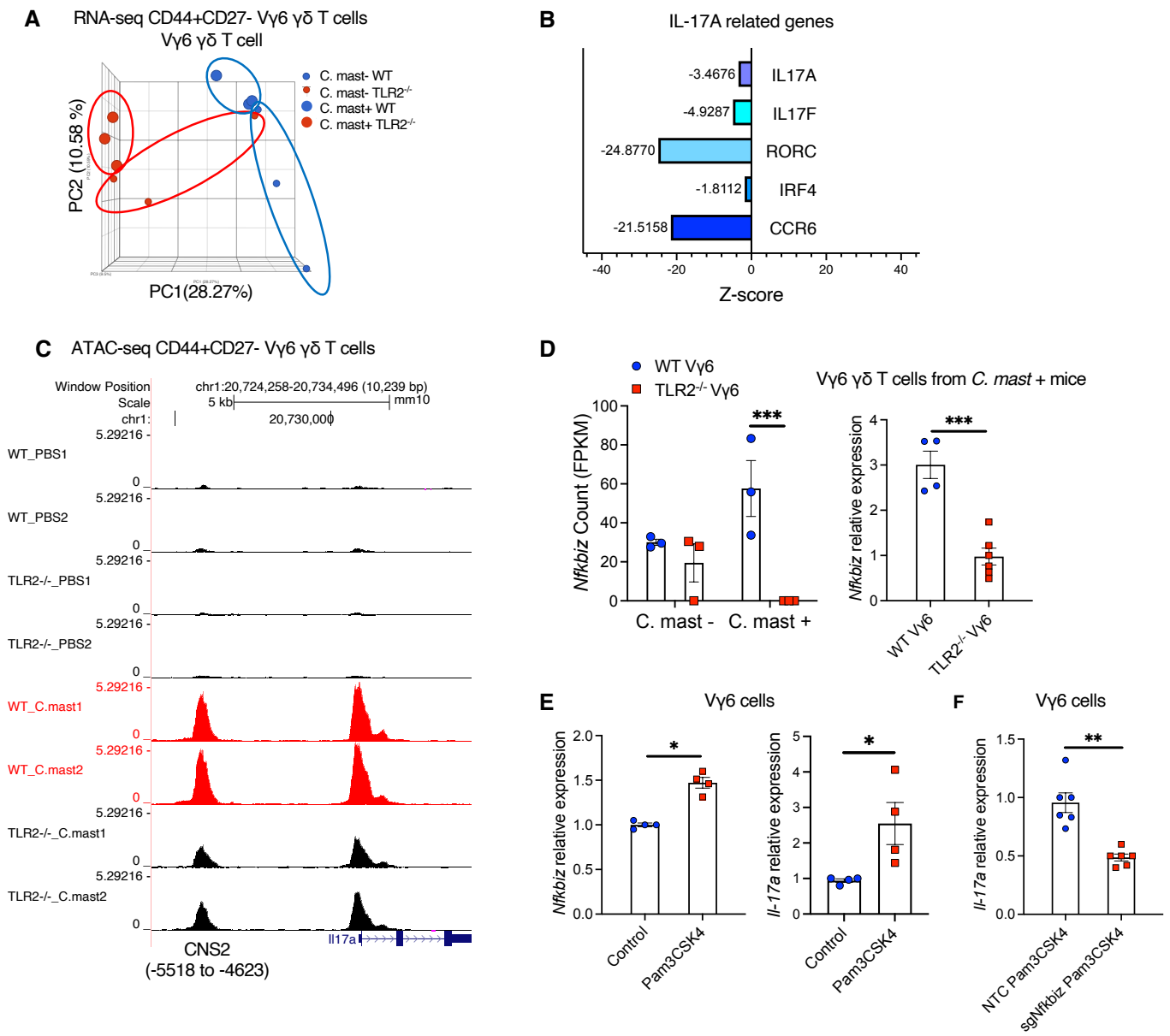

Figure 5. Compromised IL-17A response in TLR2-deficient Vγ6 cells is due to reduced expression of IκBζ

TLR2$^{-/-}$ or WT mice were associated with *C. mast* on their ocular surface.
(A) RNA-seq was performed on Vγ6 T cells isolated from the indicated mice. The PCA plot shows 4 groups: cells from naïve WT or TLR2$^{-/-}$ mice, and cells from *C. mast*$^{+}$ WT or TLR2$^{-/-}$ mice. N= 3 per group.
(B) Z scores of selected IL-17 pathway-related genes in WT and TLR2$^{-/-}$ Vγ6 cells from *C. mast*$^{+}$ mice. Blue bars represent genes downregulated in TLR2$^{-/-}$ Vγ6 cells. Z scores = (mean gene counts in TLR2$^{-/-}$ *C. mast*$^{+}$ group – mean gene counts in WT *C. mast*$^{+}$ group)/ SD of corresponding WT *C. mast*+ group's counts.
(C) ATAC-seq data showing traces, to the same scale, for Il17a genomic region of CD27-CD44^{high} Vγ6 from C. mast^{+} WT and TLR2$^{-/-}$ mice. N= 2 per group.
(D) Bar plots show the reads of *nfkbiz* (encodes IκBζ) from RNA-seq of Vγ6 cells. N= 3 per group. Vγ1^{-}Vγ4^{-} cells(Vγ6)were sorted from WT and TLR2$^{-/-}$ mice after *C .mast* inoculation. The gene expression of *nfkbiz* in sorted Vγ6 cells was quantified by real-time PCR and normalized to β-actin. N= 4-6 per group.
(E) Vγ6 cells were stimulated with IL-7 alone (Control) or IL-7 plus TLR2 ligand Pam3CSK4 for 2 days. The expression of *Nfkbiz* and *Il17a* was quantified by real-time PCR and normalized to β-actin. Data were combined from 2 experiments. N=4.
(F) Vγ6 cells were transfected with pooled CRISPR ribonucleoprotein complexes, targeting different regions of Nfkbiz (sg1 and sg2) or a non-targeting control (NTC) that does not target the mouse reference genomes. Three days later, CRISPR-edited samples stimulated with PAM3CSK4 for one day were evaluated for Il-17a expression by real-time PCR. Data were combined from 2 experiments. N=6.
Bars represent mean ± SEM. Significance was determined by Welch's t-test (D-F).

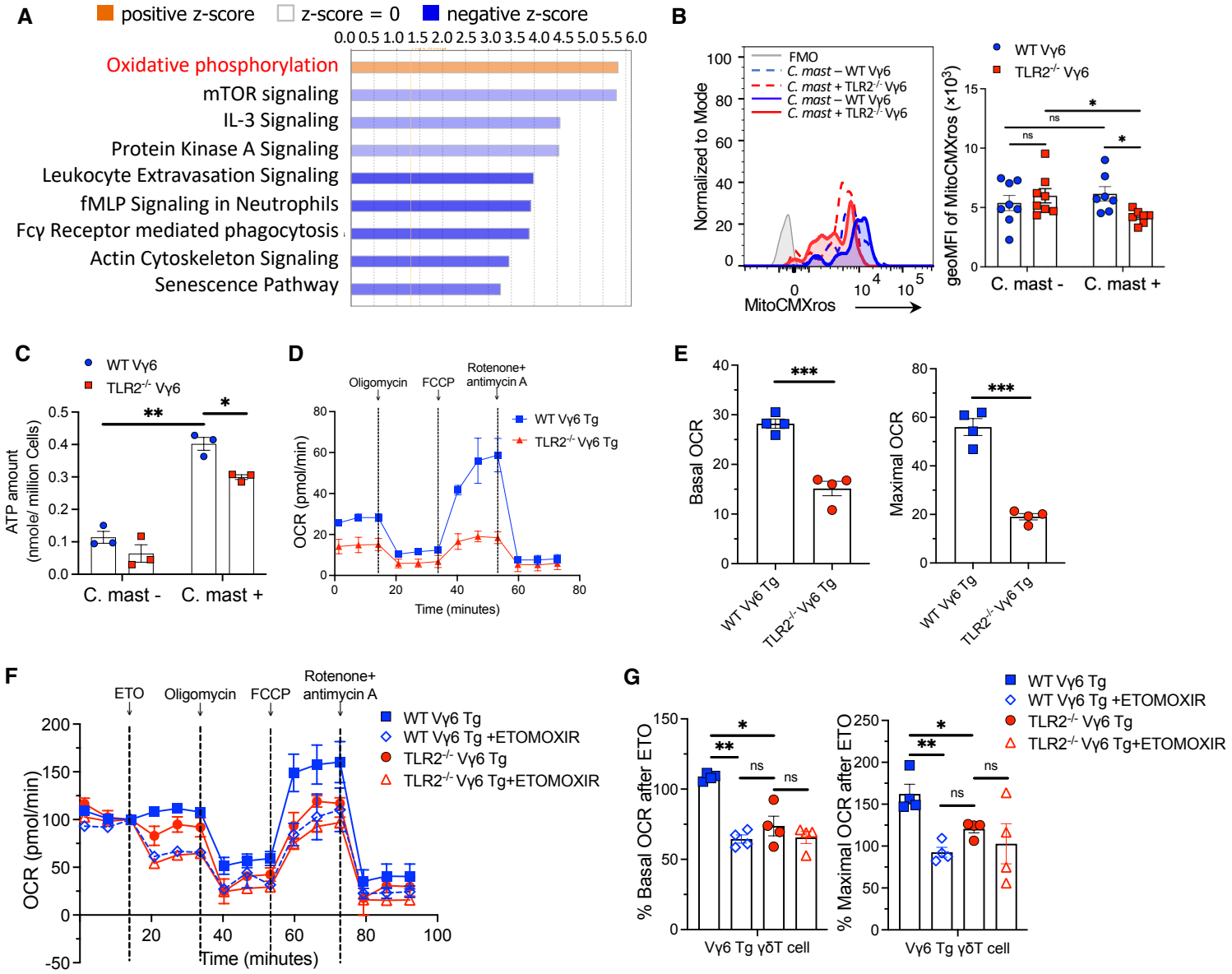

Figure 6. TLR2 deficient Vγ6 T cells show impaired FAO

γδ cells were collected from secondary lymphoid tissues of TLR2 $^{-/-}$ or WT mice and subjected to transcriptomic or Seahorse metabolic profiling.

(A) Differentially expressed genes between *C. mast*$^{+}$ WT Vγ6 T cells vs *C. mast*$^{+}$ TLR2$^{-/-}$ Vγ6 T cells were subjected to Ingenuity Pathway Analysis. Orange bars represent pathways enriched in *C. mast*$^{+}$ WT Vγ6 T cells. Blue bars represent pathways decreased in *C. mast*$^{+}$ WT Vγ6 T cells.

(B) Histogram and bar graphs showing the expression of mitochondrial membrane potential (MitoCMXros) in Vγ6 cells from WT and TLR2$^{-/-}$ mice with/without *C. mast* association. N= 8.

(C) Measurement of ATP levels in PBS and *C. mast-treated* Vγ6 cells from WT or TLR2$^{-/-}$ mice. N=3.

(D-E) OCR (oxygen consumption rate) assessment of WT and TLR2$^{-/-}$ Vγ6 T cells from *C. mast*$^{+}$ Vγ6 transgenic (Tg) mice. Cells were sorted from eye-draining lymph nodes and treated with PMA + Ionomycin for 2h before the OCR measurement. Combined data from 2 independent experiments. The OCR was measured following treatment with Oligomycin (2.5 µM), FCCP(2.5 µM), and Rotenone + antimycin A (1µM). The percentages of basal and maximal OCR after inhibitor injection were calculated and are displayed in panel **E**.

(F-G) A seahorse substrate oxidation stress test was performed in *C. mast*+ WT and TLR2$^{-/-}$ Vγ6 cells using the inhibitor ETOMOXIR. The percentages of basal and maximal OCR after inhibitor injection were calculated and are displayed in panel **G**. N= 4. Combined data from 2 independent experiments.

Significance was determined by the Whitney U test in (B-C) or Welch's t-test (E, G).

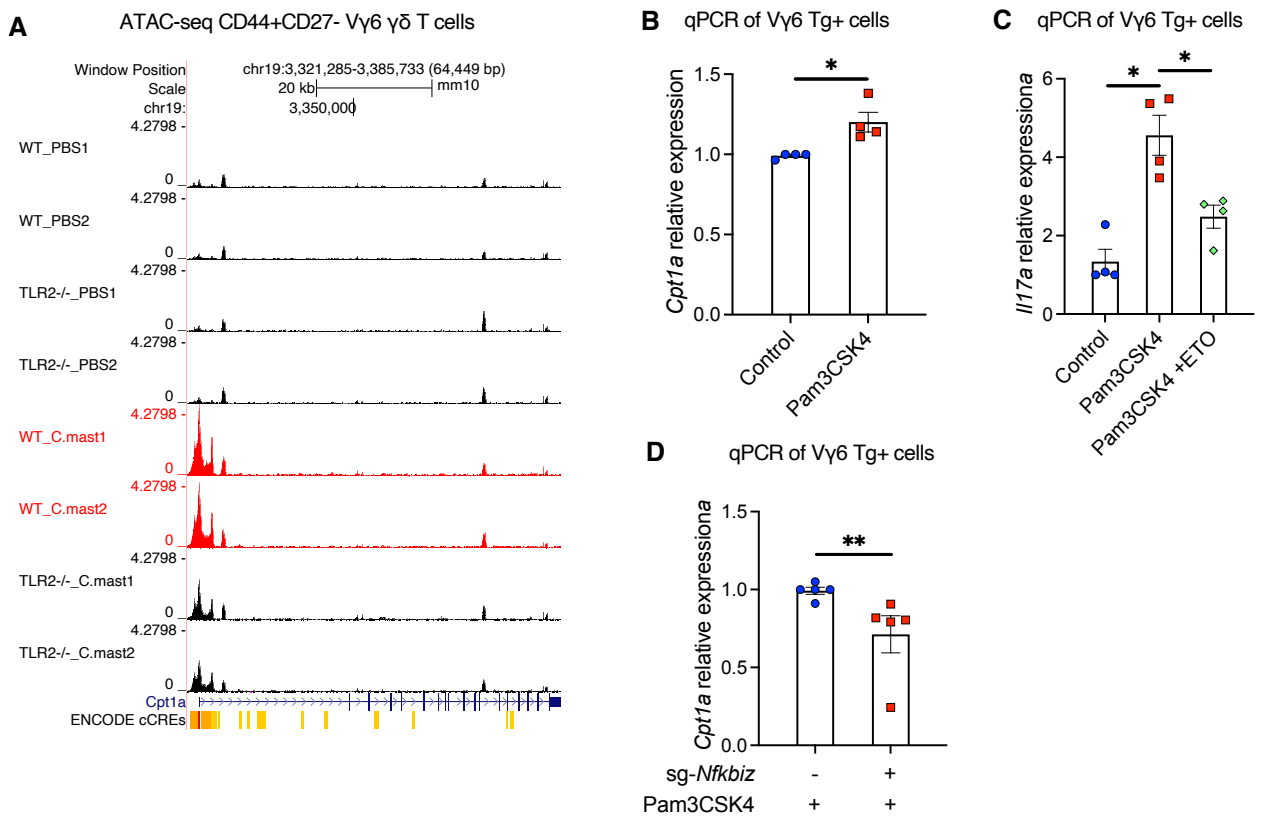

Figure 7. Impaired Cpt1 function underlines the defective IL-17A response of TLR2-deficient Vγ6 T cells

(A) UCSC genome browser output depicting ATAC-seq traces for the promoter and enhancer regions (ENCODE cCREs) of *Cpt1a* loci in CD27-CD44^{high} Vγ6 cells from WT and TLR2$^{-/-}$ mice.
(B) Vγ6 cells were sorted from *C. mast*- Vγ6 Tg mice and stimulated with IL-7 alone (Control) or IL-7 + Pam3CSK4 (Pam3CSK4) for one day. Expression of the *Cpt1a* gene is quantified by real-time PCR and normalized by the β-actin. N=4.
(C) Vγ6 cells were stimulated with IL-7 alone (Control) or IL-7 plus TLR2 ligand Pam3CSK4 (Pam3CSK4) for 2 days, Etomoxir (40 μM) was added for the final 12 hours. Expression of *Il17a* was quantified by real-time PCR and normalized to β-actin. N=4.
(D) Vγ6 cells were transfected with pooled CRISPR ribonucleoprotein complexes targeting different regions of Nfkbiz (sg1 and sg2) or anon-targeting control (NTC), not targeting mouse reference genomes. Three days later, CRISPR-edited samples were stimulated with Pam3CSK4 for one day and evaluated for *Cpt1a* expression by real-time PCR. N=5.
(B–D) Representative data of 2 independent experiments. Significance was determined by the Mann-Whitney test (B-D).